IEEE Photonics Journal
An IEEE Photonics Society Publication

Phase-Matched Mid-Infrared Difference Frequency Generation Using a Nanostructured Gallium Arsenide Metamaterial With Nanoholes

Volume 12, Number 3, June 2020

Naser A. Otman
Michael Čada

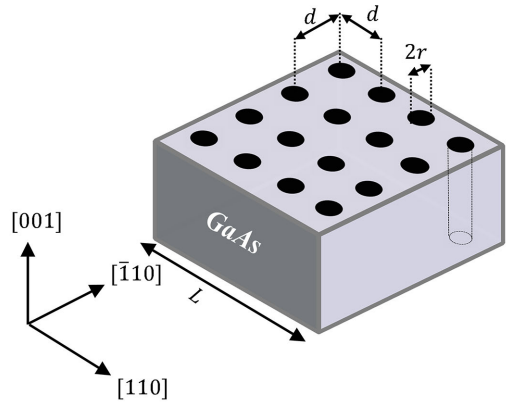

GaAs structure with nanoholes of period d and radius r. The structure has a length L along the direction of wave propagating.

DOI: 10.1109/JPHOT.2020.2992192

Phase-Matched Mid-Infrared Difference Frequency Generation Using a Nanostructured Gallium Arsenide Metamaterial With Nanoholes

Naser A. Otman [1] **and Michael Čada** [1,2]

[1]Department of Electrical and Computer Engineering, Dalhousie University, Halifax, NS B3H 4R2, Canada
[2]IT4Innovations, VSB-Technical University of Ostrava 708 33, Ostrava-Poruba, Czech Republic

DOI:10.1109/JPHOT.2020.2992192

Manuscript received November 27, 2019; revised April 16, 2020; accepted April 29, 2020. Date of publication May 4, 2020; date of current version May 26, 2020. This work was supported by the Natural Sciences and Engineering Research Council (NSERC) of Canada, and by the European Regional Development Fund of the IT4Innovations National Supercomputing Center – path to exascale project, project number CZ.02.1.01/0.0/0.0/16_013/0001791 within the Operational Programme Research, Development and Education. Corresponding author: Naser A. Otman (e-mail: naser.otman@dal.ca).

Abstract: Phase-matched wavelength conversion is achieved in difference frequency generation (DFG) in a structure of gallium arsenide (GaAs) with periodic arrays of nanoholes. Linear properties (refractive indices) of the structure are determined from the *S*-parameters of the structure. Finite difference time domain (FDTD) simulation is used to calculate the *S*-parameters. The longest wavelength achieved is 16.2229 μm and the shortest is 3.2961 μm. The results of the FDTD simulation are compared with results obtained from the effective medium theory by using the Maxwell Garnett model. The comparison shows excellent agreement.

Index Terms: Nonlinear wave mixing, metamaterials, phase matching, nanostructure.

1. Introduction

Due to the vibrational transition of many molecules, the mid-infrared (mid-IR) spectral region is an interesting area of spectroscopy. Nonlinear optical difference frequency conversion is one of the most functional techniques for generating coherent, broad, and discrete light sources for spectroscopy in the mid-IR region [1]. Mid-IR conversion via DFG involves a coupling between two waves with different frequencies to generate a difference frequency through a nonlinear medium.

Most available difference frequency generation methods based on parametric wavelength conversion use nonlinear crystals, such as periodically poled lithium niobate (PPLN), potassium titanly phosphate (KTP), and barium borate (BBO) [2], [3]. Birefringence phase matching and quasi-phase matching techniques are used to achieve efficient conversion [4]–[6]. Semiconductors, of special interest for monolithic integration, have greater optical nonlinearity properties than commonly used crystals such as PPLN, KTP, and BBO. GaAs, with its wide transparent optical window, from 1 μm to 17 μm, is the best choice for mid-infrared conversion using difference frequency generation [7]–[10]. Phase matching between the waves to be mixed is a crucial factor for strong coupling

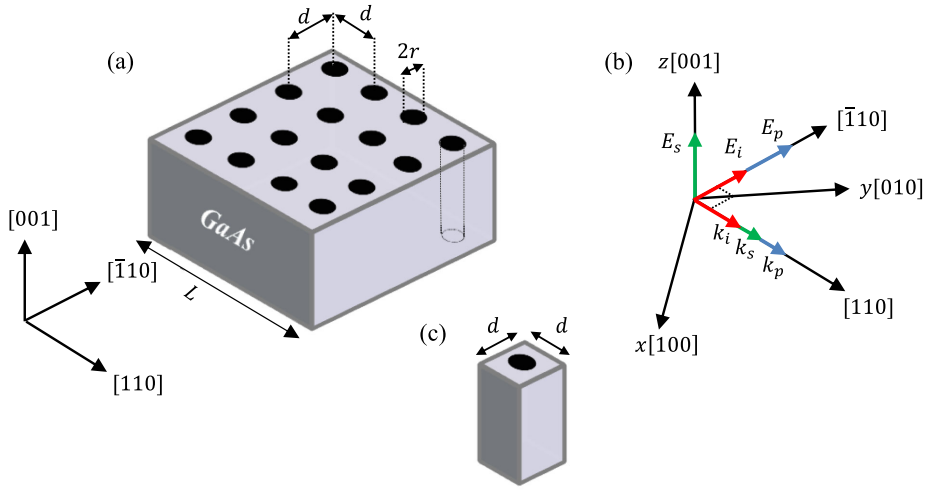

Fig. 1. (a) GaAs structure with nanoholes of period *d* and radius *r*. The structure has a length *L* along the direction of wave propagating. (b) Illustration of Miller indices of the GaAs lattice structure with Cartesian coordinates, wave propagation directions, and polarizations. (c) Unit cell of the structure.

and efficient frequency conversion. Unfortunately, it is not possible to achieve phase matching for DFG in GaAs, due to its natural isotropic properties. This problem can be solved via a multilayered structure of GaAs with other materials. Different approaches to achieve phase matching in GaAs structures include quasi-phase matching [11], [12], modal phase matching [13], [14], Bessel laser beam phase matching [15], and suspended GaAs waveguides [16].

Birefringence phase matching based on artificial anisotropy properties is possible. Artificial anisotropy properties in semiconductors were first proposed with multilayered GaAs/AlAs [17], and relatively large birefringence has been demonstrated for a multilayered GaAs/AlAs structure [18]–[20]. Tunable wavelengths from 6.7 μm to 12.7 μm using quasi-phase matching have been demonstrated in orientation-patterned GaAs [21]. Wavelengths from 7.5 μm to 8.5 μm were generated through a multilayered AlGaAs waveguide [22]. Phase-matched difference generated wavelengths from 2.8 μm to 11 μm have been achieved by using artificial birefringence in a structure of GaAs with silver nanowires [23].

In this work, we present a determination of wide, phase-matched, mid-IR generation in a structure of GaAs with nanoholes. FDTD simulation with the RSoft tool is used to calculate the scattering (*S*) parameters of the structure. Refractive indices are determined from the *S*-parameters by using a retrieving algorithm. This type of structure can be fabricated via a metal-assisted chemical etching technique [24]–[26].

2. Wave mixing and phase mismatch

Difference frequency generation employs the difference in frequency of two waves applied through an optical nonlinear medium. The two waves are defined as a pump wave of frequency $\boldsymbol{\omega_p}$, electric field $\boldsymbol{E_p}$, and wave vector $\boldsymbol{k_p}$, and a signal wave of frequency $\boldsymbol{\omega_s}$, electric field $\boldsymbol{E_s}$,and wave vector $\boldsymbol{k_s}$. The difference frequency wave that is generated is referred to as an idler wave of frequency $\boldsymbol{\omega_i}$, electric field $\boldsymbol{E_i}$, and wave vector $\boldsymbol{k_i}$, where $\boldsymbol{\omega_p > \omega_s > \omega_i}$. In this study, the nonlinear medium used is a nanostructured GaAs metamaterial with two-dimensional square arrays of cylindrical nanoholes, with period **d** and radius ***r***, as shown in Fig. 1(a). The structure has a length ***L*** along the direction of wave propagation. Fig. 1(b) shows the wave propagation directions $\boldsymbol{k_p}$, $\boldsymbol{k_s}$, and $\boldsymbol{k_i}$, and the polarization orientations of the waves with respect to the GaAs crystal axes. The basic unit cell of the structure is illustrated in Fig. 1(c).

By considering the colinear wave vectors of the interacting waves and accordance with the conservation laws of energy and momentum of the photons, $\omega_i = \omega_p - \omega_s$ and $k_i = k_p - k_s$, respectively, the colinear phase mismatching is defined as

$$\Delta k = n_p \frac{\omega_p}{c} - n_s \frac{\omega_s}{c} - n_i \frac{\omega_i}{c} \tag{1}$$

where $k_p = n_p \frac{\omega_p}{c}$, $k_s = n_s \frac{\omega_s}{c}$, and $k_i = n_i \frac{\omega_i}{c}$. n_p, n_s, and n_i are the refractive indices at the frequencies ω_p, ω_s, and ω_i, respectively. Based on this structure, only type-II coupling interaction satisfies the phase matching condition. Type-II coupling is a polarization configuration where the signal and idler polarizations are orthogonal; while in type-I, the signal and the idler polarizations are parallel. Based on type-II polarizations, we consider the applied waves at normal incidence to the holes, with electric field polarized parallel($E_\parallel$) to the holes along [001] for the signal wave E_s, and polarized orthogonal ($E_\perp$)to the holes along [$\bar{1}$10] for the pump wave E_p. Based on nonzero elements of second-order susceptibilities of GaAs $\chi^{(2)}_{xyz} = \chi^{(2)}_{yzx} = \chi^{(2)}_{zxy}$ [35], the resultant difference wave of electric field E_i will be polarized orthogonal to the holes along [$\bar{1}$10]. The three waves propagate in the plane xy, making an angle of 45° with respect to the x and y axes. The orthogonal polarizations waves have the electric field oriented parallel to the xy plane, which thus has components in x the and y directions.

It is essential to know the effective refractive indices of a structure in order to determine the phase matching. There are two main approaches for finding the effective refractive indices of metamaterial structures. The first is to use effective medium theories [27], where the long wavelength limit should be satisfied. The second is to retrieve the refractive indices from the *S*-parameters [28], [29], or from the reflection and transmission coefficients [30]. In this work, the retrieving technique is the main method employed, while the effective medium theory is used for comparison purposes.

3. Computing linear properties of the structure from S-parameters by using the retrieval technique

Full wave simulation using FDTD is applied to determine the *S*-parameters of the structure. To find the *S*-parameters of a metamaterial structure via full wave simulation, it is necessary to use a thin slab of the structure and to characterize it as an effective homogeneous medium [27]–[29]. If the structure is periodic, usually a single cell is selected as the thinnest slab. For an incident plane wave normal to the structure, the *S*-parameters are related to the refractive index n in accordance with the following equations [29]:

$$Re\,(n) = \pm Re\left\{\frac{1}{kL}cos^{-1}\left(\frac{1}{2S_{21}^2}\left[1 - S_{11}^2 + S_{21}^2\right]\right)\right\} + \frac{2m\pi}{kL} \tag{2}$$

$$Im\,(n) = \pm Im\left\{\frac{1}{kL}cos^{-1}\left(\frac{1}{2S_{21}^2}\left[1 - S_{11}^2 + S_{21}^2\right]\right)\right\} \tag{3}$$

Here L is the slab length, where $L = d$ if a single cell is considered. k is the wave number of the incident wave in free space and m is an integer number. Due to the symmetry properties of the slab, $S_{22} = S_{11}$and $S_{12} = S_{21}$. Because the structure is passive, with no negative index elements, the signs in (2) and (3) are determined so as to obtain positive real and imaginary values. Based on the long wavelength limit for metamaterials ($d,\ r \ll \lambda$) and achieving phase matching, the hole periods are almost in the range between $d = 115$ nm to 140 nm and the corresponding hole radius between $r = 0.1\ d$ to $0.25\ d$.

The *S*-parameters are computed by using a FDTD simulation of a thin one-cell layer of the structure, for incident waves polarized parallel and orthogonal to the holes, in the entire spectrum of the GaAs optical transmission window, $\lambda = 1\ \mu$m to 17 μm. Transverse periodic boundary conditions were applied in the direction perpendicular to the propagation direction of the incident waves. Experimentally measured data for the refractive index of GaAs [7] were used in the FDTD

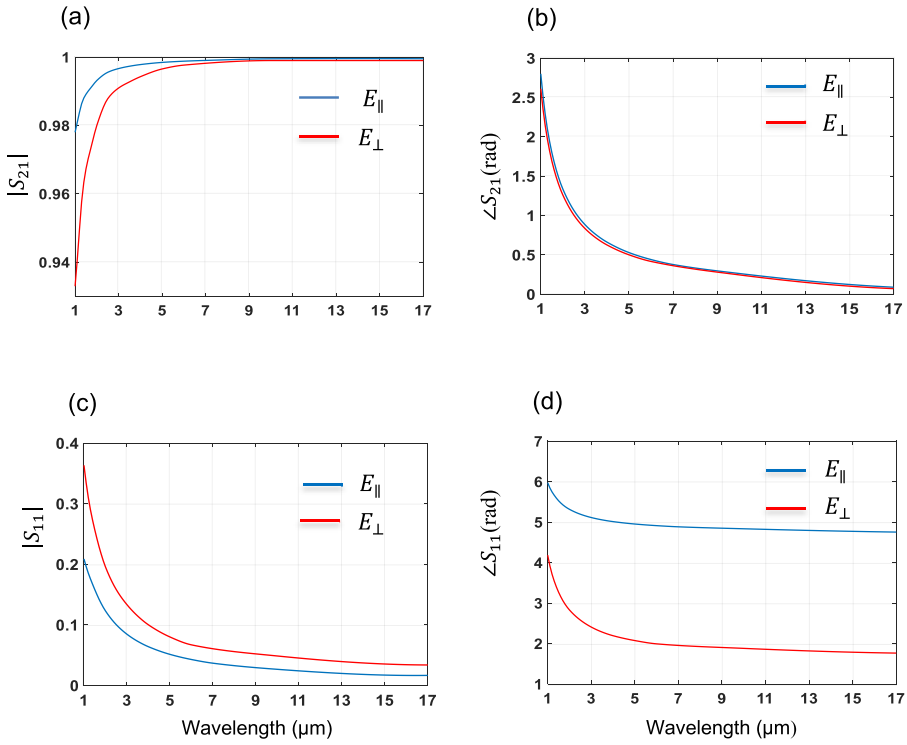

Fig. 2. S-parameters at $d = 140$ nm and $r = 35$ nm, for parallel polarization $E_\parallel$ and orthogonal polarization $E_\perp$. (a) Magnitude of S_{21}. (b) Phase of S_{21}. (c) Magnitude of S_{11}. (d) Phase of S_{11}.

simulation. Fig. 2 shows computed S-parameters of the structure, magnitude and phase, for the period $d = 140$ nm and radius $r = 35$ nm. The structure exhibits slightly more reflection with orthogonal polarization than parallel polarization, and greater transmission with parallel polarization than orthogonal polarization. As the wavelength increases, the transmission increases and the reflection decreases.

Fig. 3 shows the S-parameters, magnitude and phase, as a function of r at $\lambda = 1$ μm for two different periods: $d = 120$ nm and 140 nm.

Since GaAs is nonadsorbing in its optical window, only real indices of the structure exist. Fig. 4 shows two retrieved real indices, $Re(n^{\parallel})$ and $Re(n^{\perp})$, computed from the S-parameters presented in Fig. 2. $Re(n^{\parallel})$ represents the index parallel to the longitudinal axis of the nanoholes, and $Re(n^{\perp})$ represents the index perpendicular to the longitudinal axis of the nanoholes. The contrast between the indices, $Re(n^{\parallel})$ and $Re(n^{\perp})$ indicates that GaAs with nanoholes acts as an anisotropic medium. This promises well for birefringence phase matching in the structure.

Varying the parameters of the structure, d or r, will not change the refractive index profiles shown in Fig. 4; however, the values will be changed. Lowering the values of the indices relative to the GaAs index can be done by increasing the volume fraction of the nanoholes inside the structure. This can be achieved either by decreasing d or increasing r. Figs 5(a) and (b) show the refractive indices of the structure in relation to the GaAs index, for two different periods: $d = 120$ nm and 140 nm, and a radius of $r = 35$ nm.

4. Achieving birefringence phase matching in the structure

Changing the optical properties of GaAs from isotropic to anisotropic through the inclusion of nanoholes is beneficial, since it permits the use of birefringence phase matching in the GaAs medium. The structure was tested for phase matching possibilities by varying the pump frequency,

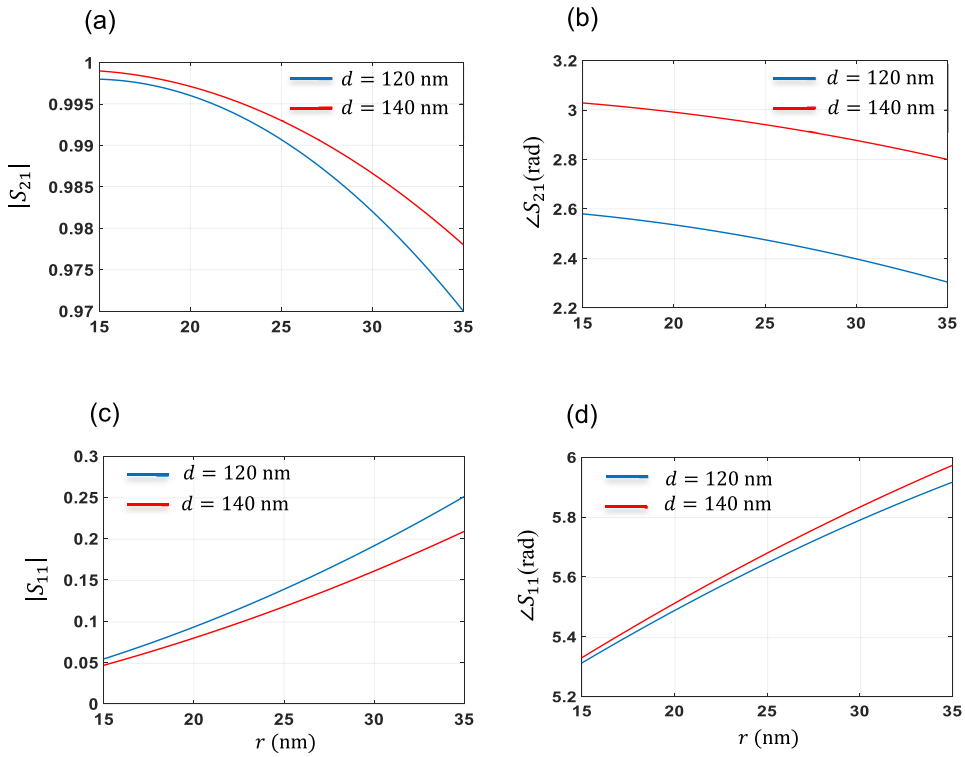

Fig. 3. *S*-parameters as a function of r for parallel polarization $E_{\|}$ at $\lambda = 1$ μm, for $d = 120$ nm and 140 μm. (a) Magnitude of S_{21}, (b) Phase of S_{21}, (c) Magnitude of S_{11}, and (d) Phase of S_{11}.

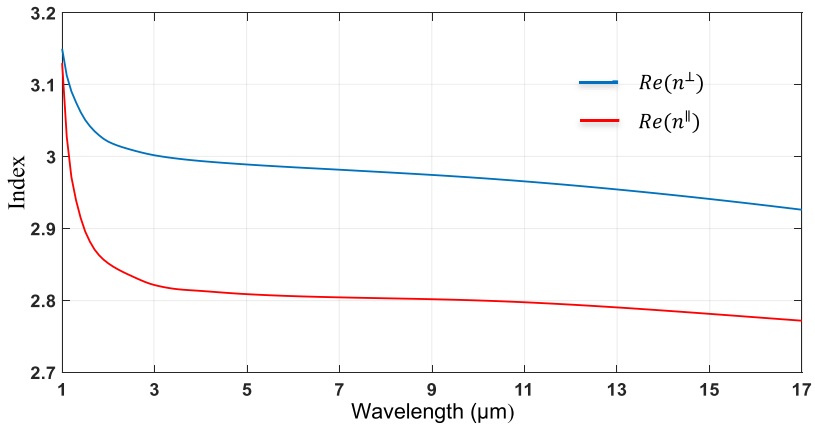

Fig. 4. Real refractive indices $Re(n^{\|})$ and $Re(n^{\perp})$ at $d = 140$ nm and $r = 35$ nm.

ω_p, and the signal frequency, ω_s. The difference frequency, ω_i, is assigned in accordance with energy and momentum conservation laws. The refractive indices plotted in Fig. 4 were applied in the phase mismatching relation given in (1). n_p and n_i correspond to the perpendicular index $n^{\perp}$, and n_s to the parallel index $n^{\|}$. Fig. 6 plots the mismatch function $(\Delta k/k_p)$ for three different pump wavelengths: $\lambda_p = 1.0333$ μm, 1.1171 μm, and 1.3053 μm. k_p is the wave number of the pump wave at the selected λ_p. Each plot satisfies the energy conservation law. Momentum conservation is

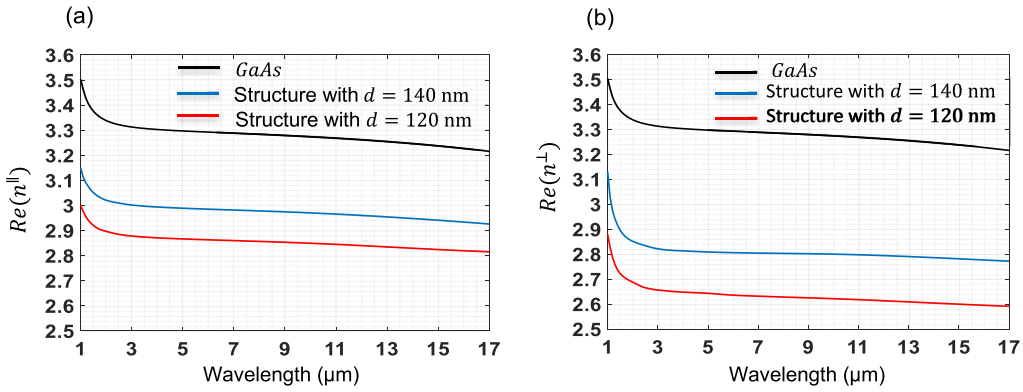

Fig. 5. Real retrieved indices at $r = 35$ nm for periods $d = 120$ and 140 nm compared with GaAs refractive index. (a) Parallel index $Re(n^{\parallel})$. (b) Perpendicular index $Re(n^{\perp})$.

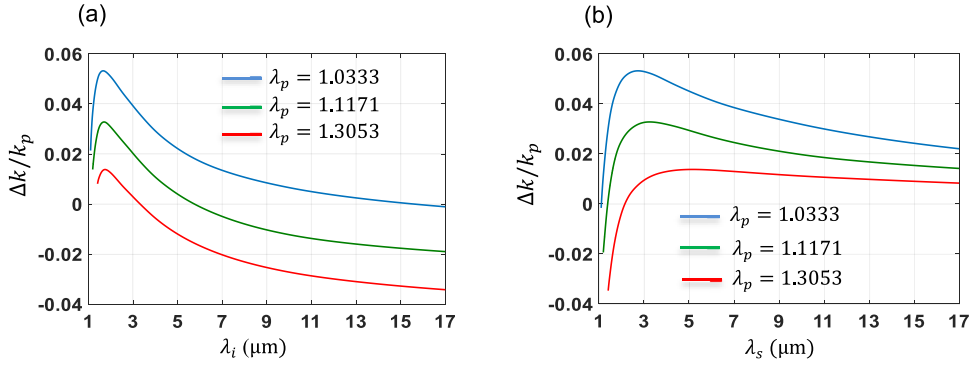

Fig. 6. Mismatch function $(\Delta k/k_p)$ for three different pump wavelengths: $\lambda_p = 1.0333$ μm, 1.1171 μm, and 1.3053 μm, at $d = 140$ nm and $r = 35$ nm. (a) $(\Delta k/k_p)$ as a function of the idler wavelength, λ_i, with phase-matched idler wavelengths: $\lambda_i = 15.5875$ μm, 5.7537 μm, and 3.3195 μm. (b) $(\Delta k/k_p)$ as a function of the signal wavelength, λ_s, with the corresponding phase-matched signal wavelengths: $\lambda_s = 1.067$ μm, 1.3863 μm, and 2.1511 μm.

satisfied at phase matching ($\Delta k = 0$). Figs 6(a) and 6(b) plot $(\Delta k/k_p)$ as a function of the idler wavelength, λ_i, and the signal wavelength, λ_s, respectively, at the specified pump wavelengths, λ_p. For these selected cases, the idler wavelengths at phase matching are $\lambda_i = 15.5875$ μm, 5.7537 μm, and 3.3195 μm, and the corresponding signal wavelengths are $\lambda_s = 1.067$ μm, 1.3863 μm, and 2.1511 μm, respectively. The structure was scanned for the entire GaAs transmission spectrum, from $\lambda = 1$ μm to $\lambda = 17$ μm. The phase-matched wavelength curves, or tuning curves, that relate the three wavelengths λ_p, λ_s, and λ_i, are shown in Fig. 7.

The tuning curves in Fig. 7 show that the pump wavelength, λ_p, extends from 1.0333 μm to 1.3983 μm. The signal wavelength, λ_s, ranges from 1.1067 μm to 2.7932 μm, and the idler wavelength, λ_i, ranges from 15.5875 μm to 2.8001 μm. This generated idler wavelength band is broad, continuous, and tunable through tuning of the input pump and/or signal wavelengths. The band can be redshifted or broadened by increasing d or decreasing r, or vice versa.

Fig. 8 shows different phase-matched wavelength curves, or tuning curves, for idler and signal wavelengths as a function of the pump wavelength, at different values of r and d. The curves for different r and d values are plotted in different colors, while the idler wavelength curves are represented by dashed lines and the signal wavelength curves by solid lines. As r decreases,

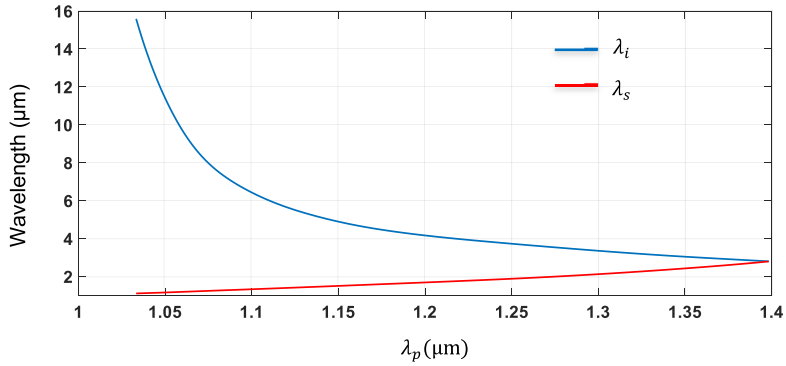

Fig. 7. Phase-matched wavelength curves, or tuning curves, that relate idler wavelengths, λ_i, and signal wavelengths, λ_s to pump wavelengths, λ_p, at $d = 140$ nm and $r = 35$ nm.

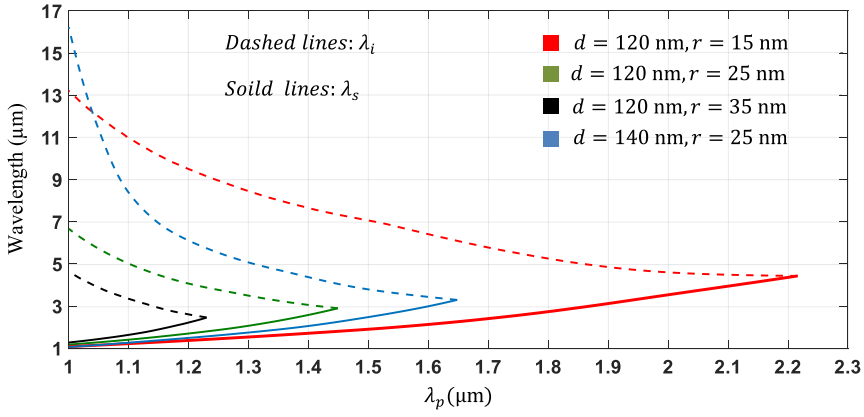

Fig. 8. Phase-matched wavelength curves that relate λ_i and λ_s to λ_p, at different values of d and r. The signal wavelengths, λ_s, are represented by solid lines, while the idler wavelengths, λ_i, are represented by dashed lines. The colors red, green, and black correspond to $d = 120$ nm with $r = 15$ nm, 25 nm, and 35 nm, respectively. The blue corresponds to $d = 140$ nm with $r = 25$ nm.

the idler and signal wavelengths are broadened and redshifted. For example, for $d = 120$ nm and $r = 35$ nm (shown in black), the longest idler wavelength is 4.633 μm and the shortest is 2.4612 μm. However, if r is decreased to 25 nm, with d remaining at 120 nm (shown in green), the longest idler wavelength is 6.6704 μm and the shortest is 2.8993 μm.

The idler wavelengths are broadened considerably more by an increase in d than by a decrease in r, as shown by the green and blue dashed curves, which correspond to $d = 120$ nm and 140 nm, respectively, with r remaining constant at 25 nm. At $d = 140$ nm, the longest idler wavelength is 16.2229 μm, as compared to 6.6704 μm at $d = 120$ nm.

5. Comparison with effective medium theory results

Effective medium theory provides a permittivity mixing formula that uses a quasi-static approximation approach to find the effective permittivity of a composite structure consisting of particles of different materials. In this study the Maxwell Garnett approximation was used to determine the effective permittivities parallel to, $\varepsilon_{\parallel}^{eff}$, and perpendicular to, $\varepsilon_{\perp}^{eff}$, the nanoholes of the structure illustrated in Fig. 1(a). To consider the two components of the metamaterial: GaAs and nanoholes,

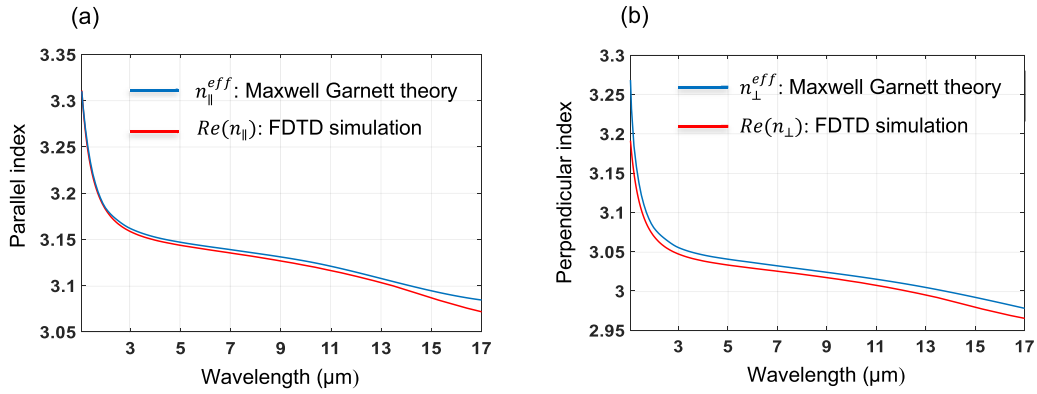

Fig. 9. Comparison of refractive indices obtained from the FDTD simulation and the Maxwell Garnett theory. (a) and (b) Parallel and perpendicular indices, respectively, at $d = 140$ nm and $r = 25$ nm for the FDTD simulation, and at the corresponding $f = 0.1002$ for the Maxwell Garnett theory.

the following Maxwell Garnett formulas were used [33], [34]:

$$\varepsilon_{\parallel}^{eff} = f + (1 - f)\,\varepsilon \tag{4a}$$

$$\varepsilon_{\perp}^{eff} = \varepsilon + \frac{2f\varepsilon\ (1 - \varepsilon)}{2\varepsilon\ + (1 - f)\,(1 - \varepsilon\ )} \tag{4b}$$

Here $f$is the volume fraction of the nanoholes included in the GaAs medium, where $0 \leq f \leq 1$, $f = \pi r^2/d^2$, and ε is the permittivity of the GaAs. The experimental data used for the GaAs refractive index [7] were the same as those used in the FDTD simulation. In order to examine the phase matching aspect, it is necessary to take into account the effective refractive indices, $n_{\parallel}^{eff} = Re(\pm\sqrt{\varepsilon_{\parallel}^{eff}})$ and $n_{\perp}^{eff} = Re(\pm\sqrt{\varepsilon_{\perp}^{eff}})$. The square root has two possible solutions, positive and negative (corresponding to a negative refractive index). Because the structure does not include any negative index materials, the positive solution was selected. Fig. 9 compares the refractive indices obtained by using the FDTD simulation with those obtained via the Maxwell Garnett theory. One set of parameters was chosen to show: $d = 140$ nm with $r = 25$ nm for the FDTD simulation and the corresponding $f = 0.1002$ for the Maxwell Garnett.

The comparison shows good agreement in the profiles, with slight disagreement in the magnitudes, seen slightly more for the perpendicular index. This slight disagreement is due to the fact that the Maxwell Garnett theory uses the proximation of the quasi-static approach while FDTD is full wave simulation.

6. Conclusions

The phase matching condition for DFG hast been investigated by using a nonlinear optical structure comprised of a GaAs with inclusions of periodic arrays of nanoholes. This structure, to our knowledge, has never been investigated for phase matching. FDTD simulation was used to determine the scattering (S) parameters of the composite structure. Linear properties (refractive indices) of the structure were then extracted from the S-parameters by using a retrieving algorithm. The structure exhibits optical anisotropy along the principal axes.

Phase matching was found at certain range of hole periods, from $\mathbf{d} = 115$ **nm** to 140 **n**, and at the corresponding radius from $\boldsymbol{r} = 0.1\mathbf{d}$ to $0.25\mathbf{d}$. The generated mid-IR is broad and tunable through tuning of the input pump and/or signal wavelengths. The generated phase matched spectrum from 3.2961 μm to 16.2229 μm was achieved at $\mathbf{d} = 140$ **nm** and $\boldsymbol{r} = 25$ **nm**. The pump

and signal wavelengths are in the spectral range less than 3 μm. For comparison with the FDTD simulation results, the Maxwell Garnett theory was used to determine effective permittivities, the comparison shows an excellent agreement.

Acknowledgment

We would like to acknowledge CMC Microsystems for providing the RSoft Component Design Suite that facilitated this research.

References

[1] Schliesser, N. Picqué, and T. W. Häns, "Mid-infrared frequency combs," *Nature Photon.*, Vol. 6, 440–449 (2012).
[2] S. J. Wagner *et al.*," Difference frequency generation by quasi-phase matching in periodically intermixed semiconductor superlattice waveguides," *IEEE J. Quantum Electron.*, Vol. 47(6), 834–840 (2011).
[3] M. Cada, J. He, R. Normandin, H. Dai, and S. Janz, "Optical nonlinear devices," *Int. J. Nonlinear Opt. Phys.*, 3, 2 (1994).
[4] J. D. Bierlein and H. Vanherzeele, *J. Opt. Soc. Am. B.* 6(4), 622–633 (1989).
[5] U. Heitmann, M. Kotteritzsch, S. Heitz, and A. Hese, *Appl. Phys. B.* 55, 419–423 (1992).
[6] L. E. Myers, R. C. Eckardt, M. M. Fejer, R. L. Byer, W. R. Bosenberg, and J. W. Pierce, *J. Opt. Soc. Am. B.* 12(11), 2102–2116 (1995).
[7] T. Skauli *et al.*, "Improved dispersion relations for GaAs and applications to nonlinear optics," *J. Appl. Phys.*, vol. 94, no. 10,pp. 6447–6455, 2003.
[8] M. Cada, "Nonlinaer optical devices," *Invited Paper, Optica Pura y Aplicada*, Vol. 38(3) (2005).
[9] M. Cada, "Optical harmonic mixers," *IEEE J. Quantum Electron.*, 31, 269 (1995).
[10] S. Helmy *et al.*, "Recent advances in phase matching of second-order nonlinearities in monolithic semiconductor waveguides," *Laser Photon. Rev.*, Vol. 5(2) (2010).
[11] S. J. B. Yoo, C. Caneau, R. Bhat, M. A. Koza, A. Rajhel, and N. Antoniades, "Wavelength conversion by difference frequency generation in AlGaAs waveguides with periodic domain inversion achieved by wafer bonding," *Appl. Phys. Lett.*, 68, 2609 (1996).
[12] Grisard, E. Lallier, and B. Gérard, "Quasi-phase-matched gallium arsenide for versatile mid-infrared frequency conversion," *Opt. Mater. Express*, Vol. 2(8) (2012).
[13] K. Moutzouris *et al., Appl. Phys. Lett.* 83(4), 620–622 (2003).
[14] S. Ducci, L. Lanco, V. Berger, A. De Rossi, V. Ortiz, and M. Calligaro, *Appl. Phys. Lett.* 84(16), 2974–2976 (2004).
[15] P. Liu, W. Shi, D. Xu, X. Zhang, G. Zhang, and J. Yao, "Efficient phase-matching for difference frequency generation with pump of Bessel laser beams," *Opt. Express*, Vol. 24(2) (2016).
[16] T. H. Stievater *et al.*, "Mid-infrared difference-frequency generation in suspended GaAs waveguides," *Opt. Lett.*, Vol. 39(4) (2014).
[17] J. P. van der Ziel, M. Ilegems, and R. M. Mikulyak, "Optical birefringence of thin GaAs-AlAs multilayer films," *Appl. Phys. Lett.*, Vol. 28(12) (1976).
[18] Fiore, V. Berger, E. Rosencher, N. Laurent, N. Vodjdani, and J. Nagle, "Huge birefringence in selectively oxidized GaAs/AlAs optical waveguides," *Appl. Phys. Lett.* 68, 1320 (1996).
[19] E. Guillotel *et al.*, "Parametric amplification in GaAs/AlOx waveguide," *Appl. Phys. Lett.*, Vol. 94(17) 1110 (2009).
[20] Fiore, V. Berger, E. Rosencher, P. Bravetti, and J. Nagle, "Phase matching using an isotropic nonlinear optical material," *Nature*, Vol. 391 (1998).
[21] P. J. Jiang *et al.*, "Wide tunable midinfrared generation in orientation -patterned GaAs pumped with a femtosecond Tm-fiber system," *Opt. Lett.*, vol. 37(14) 2928–2930, 2012.
[22] D. F. Logan, M. Giguere, A. Villeneuve, and A. S. Helmy, "Widely tunable mid-infrared generation via frequency conversion in semiconductor waveguides," *Opt. Lett.*, Vol. 38(21), 4457–4460, 2013.
[23] N. A. Otman and M. Cada, "Phase matching for difference frequency generation in GaAs via an artificial birefringence technique using silver nanowires," *IEEE Photon. J.* 10 (3), 2018, Art. no. 1300110.
[24] Y. Song, K. Choi, D.-H. Jun, and J. Oh, "Nanostructured GaAs solar cells via metal assisted chemical etching of emitter layers," *Opt. Express.* 25(20), 23862–23872 (2017).
[25] M. DeJarld *et al.*, "Formation of high aspect ratio GaAs nanostructures with metal-assisted chemical etching", *Nano Lett.* 11, 5259–5263 (2011).
[26] H. Asoh, Y Suzuki, and S. Ono, "Metal-assisted chemical etching of GaAs using Au catalyst deposited on the backside of a substrate," *Electrochimica Acta.* 183, 8–14 (2015).
[27] W. Cai and V. M. Shalaev, *Optical Metamaterials: Fundamentals and Applications* (Springer, 2009).
[28] X. Chen, T. M. Grzegorczyk, B.-I. Wu, J. Pacheco, Jr., and J. A. Kong, "Robust method to retrieve the constitutive effective parameters of metamaterials," *Physical Rev. E.* 70, 016608 (2004).
[29] D. R. Smith, D. C. Vier, Th. Koschny, and C. M. Soukoulis, "Electromagnetic parameter retrieval from inhomogeneous metamaterials," *Physical Rev. E.* 71, 036617 (2005).
[30] D. R. Smith, S. Schultz, P. Markos, and C. M. Soukoulis, "Determination of effective permittivity and permeability of metamaterials from reflection and transmission coefficients," *Physical Rev. B.* 65, 195104 (2002).
[31] Rose and D. R. Smith, "Overcoming phase mismatch in nonlinear metamaterials," *Opt. Mater. Express.* 1(7), 1232–2143 (2011).
[32] C. F. Bohren and D. R. Huffmn, *Absorption and Scattering of Light by Small Particles* (Wiley, 1983).

[33] Z. L. Mei, J. Bai, and T. J. Cui, "Gradient index metamaterials realized by drilling holes arrays," *J. Phys. D: Appl. Phys.* 43, 055404 (2010).
[34] Y. Liu, G. Bartal, and X. Zhang, "All-angle negative refraction and imaging in a bulk medium made of metallic nanowires in the visible region," *Opt. Express*, Vol. 16(20), 15439 (2008).
[35] R. Boyed, *Nonlinear Optics*, 3rd Edition (Elsevier, 2003).